Heads-on skyrmion collisions

Héctor Corte-León (leo_corte@msn.com)
National Physical Laboratory
Mehran Vafaee Khanjani
Gerhard Jakob
Johannes Gutenberg University of Mainz https://orcid.org/0000-0001-9466-0840
Mathias Kläui
Johannes Gutenberg University of Mainz https://orcid.org/0000-0002-4848-2569
Felipe Garcia-Sanchez
Istituto Nazionale di Ricerca Metrologica https://orcid.org/0000-0002-3655-4836
Craig Barton
Olga Kazakova
National Physical Laboratory https://orcid.org/0000-0002-8473-2414

Article

Keywords: MFM, skyrmion, neuromorfic, dynamics, nanoscale

Posted Date: February 3rd, 2023

DOI: https://doi.org/10.21203/rs.3.rs-2458354/v1

Abstract

Magnetic textures known as skyrmions have captured the attention of the scientific community working on magnetism for a large part of the last decade due to their potential application in novel neuromorphic devices to carry information and perform computational operations[1, 2]. This is due to the ease of manipulation with electrical currents, and the stability of individual skyrmions against interactions with defects or other skyrmions. Now, while there are plenty of reports on skyrmion manipulation using electrical currents, there are very few studies of skyrmion-to-skyrmion interactions (i.e. skyrmion collisions). While there have recently been studies on skyrmion lattices to extract the interaction potential[3, 4], a more direct approach is to manipulate individual skyrmions directly, which however has been challenging so far. The reason for that is that very few tools allow for manipulating skyrmions individually and with enough precision to cause collisions in a controllable and repeatable way. In here, we show how using magnetic force microscopy (MFM), and the field gradient produced by MFM probes, it is possible to visualize skyrmions, manipulate them, and create skyrmion collisions to study skyrmion-to-skyrmion interactions or investigate the role of pinning at material defects.

1. Introduction

Going beyond the current paradigm in computation, into the realm of neuromorphic computing, requires of novel electronic elements that can mimic the behavior of neurons, and operate with very low power consumption[5]. It is for this reason that devices such as artificial neurons based on magnetic skyrmions have been proposed[6, 7].

The fundamental principle at operation in such devices is that a skyrmion moves inside of a magnetic element, and its position modifies the electrical properties (e.g. resistance) of the overall device. Skyrmions are topologically stabilized magnetic textures that can have both polarity and chirality, and that move inside of the material that host them in a particle-like manner. Multilayer systems with broken symmetry can host skyrmions, because the coupling between layer gives raise to Dzyaloshinskii-Moriya interaction (DMI)[8–10], which makes energetically favorable arrangements of the magnetization where the spin twist from one position to another.

The ease of manipulation of skyrmions with electrical currents, in comparison with other magnetic elements, e.g. domain walls[11], has prompted a large number of reports on manipulation of skyrmions using electrical currents[12–18]. In particular, the smaller power required, has shifted the attention towards skyrmions-based neuromorphic devices[7]. However, undesired effects appear when manipulating skyrmions with current, and they are difficult to study because of the very nature of the manipulation using current (i.e. when several skyrmions are present, it is very difficult to control each individually), example of these are pinning of skyrmions on defects[10, 19], and skyrmions-to-skyrmion interactions[3, 4].

In here, building up on previous results[20–22] that demonstrate how to use magnetic force microscopy[23] (MFM) to manipulate skyrmions, we show how by repeating the manipulation process it is possible to

disentangle skyrmions-to-skyrmion interactions from MFM probe-skyrmion interactions, and how by doing that it is possible to study pinning at defects, and skyrmions-to-skyrmion interactions.

2. Results

The material used to host skyrmions is a multilayer thin film with the composition Ta(5.7) [Pt(3.4)/CoFeB(0.8)/MgO(1.4)]x15 Ta(5) (thickness in nm). It has perpendicular anisotropy which results in meander-like domains, and hosts skyrmions when a biasing magnetic field is applied. It was studied in another article[20], where it was determined that it has a Dzyaloshinskii-Moriya interaction (DMI) value of $|D| = 1.0 \pm 0.1 \mathrm{mJ/m^2}$.

2.1. Imaging and manipulation using MFM

In a previous publication[20], it has been shown a method to manipulate skyrmions in thin films with an applied magnetic field and the aid of MFM. The method, which will be used here, consists in saturating the sample with 1-2T of in-plane field[1, 24], as depicted in Fig. 1(a). This step is known to facilitate the nucleation of skyrmions later on, when applying an out-of-plane field. The next step consists in imaging the sample's surface, i.e. topography, without applying magnetic field, in non-contact mode, as shown in Fig. 1(b). Then the MFM probe is lift from the surface, Fig. 1(c), and the external out-of-plane field is raised to the value where skyrmions start to appear (~ 65 mT in our case). Without reducing the applied magnetic field, magnetization is imaged in lift mode (i.e. phase contrast), using the topography recorded at the beginning as a reference. In this way, because the probe images at a distance, without coming close enough to the surface to cause interference, it is possible to image skyrmions, without disturbing them significantly.

Note that after the initial in-plane saturation, the field applied to the sample never exceeds ~ 70 mT of field (either in-plane or out-of-plane).

Also, it is important to note that because there is no real-time feedback correcting the drift of the sample in the z direction (in a working day we observed a drift of less than 20 nm in the x-y plane), manual correction is needed. This was done by the user judging from the contrast of the image when the probe needed raising or lowering to compensate the sample drift.

The next step in the process is the actual manipulation of the magnetization in the sample. This is done by reducing the distance between the probe and the sample and scanning the desired area in semi contact mode, as shown in Fig. 1(e). The process then continues alternating between imaging, Fig. 1(d), and writing, Fig. 1(e), until achieving the desired magnetization configuration.

It is worth mentioning here, that while MFM imaging is most sensitive to field gradients directly underneath the probe (named "sensing point" in Fig. 1(f)), the interaction between the probe and the skyrmions is more likely to happen at a different point (named "writing point"). This is due to the relative position of probe and skyrmions changing between imaging and writing (i.e. probe closer to the surface),

because the skyrmion could be more affected by in-plane field rather than out-of-plane (or vice versa), and asymmetries in the probe's shape. In addition, the sample surface and the probe will be at some angle in respect to each other that will make the whole situation non symmetric. All this will show up in a lateral shift when pushing skyrmions from different directions or between the image of the skyrmions and when it actually starts moving by the effect of the probe.

2.2. Skyrmion collisions

Utilizing the process described in the previous section, several experiments manipulating skyrmions were carried out. A typical example of such experiments is shown in Fig. 2 (and Supplementary movie 1, both comprised of MFM images). In Fig. 2 the green zigzagging arrow indicates the area where the sample was scanned in semicontact mode to manipulate the magnetization (the arrow points towards where the scanning ends). The manipulation shown in Fig. 2 starts in Fig. 2(a) with part of the surface uniformly magnetized upwards. This was achieved by a previous step where that area was scanned in semicontact mode several times to move skyrmions away. The first step, Fig. 2(a) to (b), consists in moving several skyrmions onto the area with uniform magnetization. The doted circles are guides to track the movement of the skyrmions. Then, the rightmost skyrmion is pushed towards the left, Fig. 2(b) to (c), to check if it is pinned at a defect or free to move (as it will be discussed later on with other examples, it is free to move). Then, steps shown in Fig. 2(d) to (h) the bottom skyrmions is pushed upwards, to check if it is also pinned or not (it is not), and to place it close to the other skyrmions. The last step, Fig. 2(h) to (i), consists in pushing the left skyrmion towards the right to make it collide with the rightmost skyrmion. As a result of the collision one skyrmion bounces back and the other moves to the right. It will be discussed later on how to distinguish between skyrmion-to-skyrmion interactions and probe-to-skyrmion manipulation.

2.3. Differentiating between probe-skyrmion or skyrmions-skyrmion interactions

The writing process demonstrated above in Fig. 2 is, however, of little use if it is not possible to differentiate between skyrmion movement due to interaction with the probe, or because of the interaction with another skyrmion. To solve the issue, the data from many manipulation experiments was captured and summarized for four different MFM probes (Fig. 3 to 6, where each figure represents a different probe). Using collisions such as the one shown in Fig. 2, and repeatedly trying to move skyrmions by placing the probe at different distances, the position of skyrmions was measured before/after, as well as the minimum probe-to-skyrmion distance when performing the writing (Fig. 3(a) (i) to (iv)). To simplify the data analysis, manipulation was limited to horizontal (i.e. left and right) and vertical (i.e. up and down) directions. The insets in Fig. 3(a) (i) to (iv), indicate the relative position of the probe and the skyrmions, and which direction is taken as a positive distance.

The straight lines in Fig. 3(a), blue continuous/red dashed, represent the zero displacement, and the one-to-one relationship (i.e. the skyrmions moves as much as the distance the probe pushes it) respectively. The shaded area is then uncertainty margin of ± 75 nm estimated from the average change in position of

skyrmions between consecutive MFM images. The position of the one-to-one line (i.e. the red straight line), was obtained using least square fitting to the skyrmion motion that didn't involve collisions or pinning (i.e. using only the data of skyrmions free to move).

As mentioned before in Fig. 1(f), the sensing point and the writing points are in different locations, this can be seen as a shift in the graphs shown in Fig. 3(a). In the ideal case of sensing and writing points being in the same position, the blue and the red lines will meet at zero minimum distance, instead, depending on which direction is used to manipulate the skyrmions, the probe has to move closer to the apparent position of the skyrmions detected when performing MFM imaging (or even scan over the apparent position, when the red and blue lines meet at negative values).

From the data shown in Fig. 3(a) it is possible to identify the following cases of interest:

2.4. Skyrmion manipulation without significant pinning

The red data point highlighted in Fig. 3(a)(i), and its corresponding frames, shown in Fig. 3(b) represents the case of a skyrmions that can be manipulated and it is not pinned to defects in the thin film. This is known because the red data point lays perfectly within the boundaries of the ideal displacement (i.e. red doted line and it's 75 nm uncertainty). Note that as in Fig. 2, doted circles are guides to easy identifying which skyrmions move between frames. The coordinates of the skyrmions (shown in μm), as well as the corners of the area scanned to the probe refer to the bottom left of the image (which in some cases was cropped to fit in the figure). Further examples of skyrmion manipulation without pinning can be seen in the Supplementary movies 3 and 8.

2.5. Skyrmion pinned to defects in the film

The green and purple data points in Fig. 3(a)(i), and their corresponding frames in Fig. 3(c), correspond to a situation where the movement of a skyrmion is much less than the expected distance the probe pushed it. To corroborate that this is indeed a property of the thin film, and not a stochastic behavior due to the skyrmion-probe interaction, these two points correspond to a set of experiments trying to move the same skyrmion repeatedly (the black points in Fig. 3(a)(i) next to the purple and green data points correspond to other tries). Since in other cases the skyrmion-tip interaction gives rise to a predictable behavior, and in this case repeated writing attempts produce the same result, it has to be concluded that there is a pinning position in the material, which prevents the skyrmion from moving under the same interaction as their neighbor skyrmions.

This highlights the fact that by accumulating enough data (i.e. all the movement experiments compiled in Fig. 3 (a)(i)-(iv)), it is possible to identify pinning sites. Moreover, this shows a way of qualitatively studying defects: moving a skyrmion across all the surface and comparing its behavior to that of the "ideal" case.

2.6. Collision with a pinned skyrmion

The blue data point in Fig. 3(a)(iv), and its corresponding frames in Fig. 3(d), correspond to the case where a skyrmion collides with a pinned skyrmion (the turquois data point). As in the case of pinned skyrmion discussed before, the blue data point is well below the ideal red doted line, indicating either pinning, or as in this case, a collision with a strongly pinned skyrmion (the turquoise data point which didn't move at all). Further frames corresponding to the same manipulation can be seen in the Supplementary movie 7.

2.7. Collision with a not pinned skyrmion

On contrast to the previous case, red and blue data points in Fig. 4(a)(iv), and their corresponding frames in Fig. 4(b), corresponds to an interaction where none of the skyrmions are pinned, and thus after the collision both skyrmions move. Note that Fig. 4 corresponds to another MFM probe, but as with the previous probe, sufficient interactions were studied to be able to distinguish the ideal behavior (i.e. red dotted line), from the non-interacting situation (blue continuous line). It is possible to see in this case (red and blue data points), that both skyrmions move, the blue one bouncing back, and the red one moved forward (i.e. towards the right). Notoriously the distance that a skyrmion moved is asymmetric, however, without a knowledge of the pinning sites in the film, it is not possible to say more about this particular collision. Further collision examples can be observed in Supplementary movies 2, 5, 10, and 11.

2.8. Defects that allow skyrmions to stay in close proximity

The next is an example of how the subjacent pinning landscape can modify the skyrmion-to-skyrmion interaction to make it appear as skyrmions attract each other. Yellow and green data points in Fig. 4(a)(iv), and their corresponding frames in Fig. 4(c), corresponds to a situation where the probe tries to move the yellow skyrmion, and it is too far to move the green skyrmion. From the observed movement it can be concluded that the green skyrmion moved left, whilst the yellow skyrmion moved right, and down (the down movement is not captured in Fig. 4(a)(iv), but can be observed in Fig. 4(c)). The movement of the yellow skyrmion could be affected by the probe and the collision with the green skyrmion, thus it is very difficult to conclude anything from it (a part from the fact that it remained within the vicinity of the green skyrmion). In the case of the green skyrmion however, because the green skyrmion is initially too far away to be affected by the probe, any movement observed must be due to the interaction with the yellow skyrmion. This means that when the yellow skyrmion is moved to the right of the image, pushed by the probe, and the green skyrmion responds by moving left, it moves towards the yellow skyrmion due to the skyrmion-to-skyrmion interaction. Or to be more precise, the two skyrmions move towards each other and remain in close proximity due to the skyrmion-to-skyrmion-to-pinning landscape interaction.

This is a very important result, because it highlights that under the right circumstances, the underlying pinning energy landscape not only affects skyrmion movement (e.g. preventing skyrmions from moving, or deflecting their trajectories), it also generate conditions where it might be more energetically favorable for to skyrmions to remain in close proximity. Further frames corresponding to this manipulation can be seen in the Supplementary movie 9.

Another two examples of the effect of the underlying pinning landscape can be seen in Fig. 5. Green and blue data points in Fig. 5(a)(i), and their corresponding frames in Fig. 5(b) corresponds to a situation where three skyrmions are aligned horizontally, and the rightmost skyrmion is pushed towards the other two (i.e. left). In this case the blue skyrmion moves as much as the probe pushes it, not noticing any change in trajectory due to interactions with the other skyrmions or the pinning landscape. The green skyrmion on the other hand, which is too far away to be affected by the probe (as it can be seen in Fig. 5(a)(i) that it lays far away from the distance at which the probe starts interacting with the skyrmions), moves right as a result of the movement of the blue skyrmion. The overall movement is as if the blue and green skyrmions attract each other. However, this is just another example of the underlying pinning landscape acting on skyrmion movement and masking the real skyrmion-to-skyrmion interaction, which in these materials stacks is expected to be purely repulsive[4].

The red data point in Fig. 5(a)(i) and its corresponding frames in Fig. 5(c), represents a case where a skyrmion (red) approaches another skyrmion (turquois) which is trapped in a strong pinning potential. The pinning potential in this case is strong because not only the turquois skyrmion doesn't move, but the red skyrmion gets trapped in it as well, making it look like the red skyrmion is orbiting around the turquois one. This same behavior can be observed in the red data point in Fig. 6(a)(i) and its associated frames in Fig. 6(d). Interestingly, in the case of Fig. 6(d), it can be seen in the Supplementary movie 4, which shows the process leading to the frames shown in Fig. 6(d), that the two skyrmions move around and collide several times before getting trapped in the pinning potential that gives rise to the orbiting behavior. Further examples of skyrmions remaining in close proximity can be seen in the Supplementary movie 2.

On a similar manner, the blue data point in Fig. 6(a)(iv) and its associated frames in Fig. 6(b) also represent the collision with a strongly pinned skyrmion (the yellow skyrmion doesn't move as a result of the interaction), however, in this case the pinning is very localized and doesn't trap the second skyrmion (i.e. the blue one), which bounces back from the collision with the yellow skyrmion. Similar behavior can be seen in the Supplementary movie 7.

The last example discussed here corresponds to the purple and green data points in Fig. 6(a)(iv) and their associated frames in Fig. 6(c). This is a similar case as the one described before with three skyrmions aligned together (i.e. Figure 5(b)). However, in this case, the central skyrmion (green) does not move closer to the skyrmion being moved by the tip (purple), it moves towards the skyrmion farthest away from the tip (the turquois one). Interestingly, while the turquois and green skyrmions seems trapped in a pinning site, the purple skyrmion bounces back from the collision and moves away. This process, along with the steps leading to the alignment of the skyrmions can be seen in the Supplementary movie 6.

3. Conclusion

The results presented here demonstrate that reproducible skyrmion collisions can be generated and studied using an advanced MFM system. Moreover, by collecting the data corresponding to many interactions, it is possible to differentiate between: skyrmion movement due to tip interaction; to

skyrmion-to-skyrmion interaction; and/or due to the pinning landscape. Thus, this approach allows for the study the dynamics of such systems, and enabling the investigation of the pinning energy landscape.

In addition to demonstrating the manipulation method, a few interaction examples have been studied, demonstrating that the pinning energy landscape can obfuscate the skyrmion-to-skyrmion interaction (which is repulsive in this case), and can make skyrmions appear as if there is an attractive force between, which must be taken into account when analyzing the behavior.

4. Experimental Section

4.1. SPM imaging

The AFM imaging was performed using NT-MDT Ntegra-AURA scanning probe microscopy system. The selected probes for imaging and manipulation where MFM_LM from tips nano. These probes where used previously on the same type of sample[20] and are expected to have both low stray and coercive fields, being the dipole approximation[25] a magnetic dipole along the z direction with value between 0.8–1.65 x $10^{-16} Am^2$. Or in other words, these probes produce[25] between 1.5 and 4.8 mT of field along the z axis at a distance of 100 nm from the tip apex.

4.7. Data post-processing

The AFM files were processed using Gwyddion and Matlab. Each frame was opened in Gwyddion version 2.53.20190809, and line artefacts were corrected either using “align rows”, or manually selecting the flat areas of the image with the toll “path level”.

The frames where then loaded into Matlab as black and white images (a threshold was used in some frames to differentiate more clearly between skyrmions), then the tool “imfindcircles” was used to fit skyrmions by circles and thus track their position.

Declarations

Supporting Information

Supporting Information is available from XXX

Acknowledgements

The authors wish to thank Arianna Casiraghi for useful discussions.

The authors acknowledge the financial support from the European Metrology Programme for Innovation and Research (Grant No. 15SIB06), NanoMag. The group in Mainz acknowledges funding from TopDyn, SFB TRR 173 Spin+X (project A01 #268565370 and project B12 #268565370). The work was additionally funded by the Deutsche Forschungsgemeinschaft (DFG, German Research Foundation) Project No.

403502522 (SPP 2137 Skyrmionics). This project has received funding from the European Research Council (ERC) under the European Union's Horizon 2020 research and innovation programme under grant agreement No. 856538 (ERC-SyG 3D MAGIC).

References

1. J. Zázvorka, F. Jakobs, D. Heinze, N. Keil, S. Kromin, S. Jaiswal, K. Litzius, G. Jakob, P. Virnau, D. Pinna, K. Everschor-Sitte, L. Rózsa, A. Donges, U. Nowak, M. Kläui, *Nature Nanotechnology* **2019**, *14*, 658.
2. D. Prychynenko, M. Sitte, K. Litzius, B. Krüger, G. Bourianoff, M. Kläui, J. Sinova, K. Everschor-Sitte, *Physical Review Applied* **2018**, *9*, 014034.
3. J. Zázvorka, F. Dittrich, Y. Ge, N. Kerber, K. Raab, T. Winkler, K. Litzius, M. Veis, P. Virnau, M. Kläui, *Advanced Functional Materials* **2020**, *30*, 2004037.
4. Y. Ge, J. Rothörl, M. A. Brems, N. Kerber, R. Gruber, T. Dohi, M. Kläui, P. Virnau, **2021**.
5. J. Grollier, D. Querlioz, K. Y. Camsari, K. Everschor-Sitte, S. Fukami, M. D. Stiles, *Nature Electronics* **2020**, *3*, 360.
6. K. M. Song, J. S. Jeong, B. Pan, X. Zhang, J. Xia, S. Cha, T. E. Park, K. Kim, S. Finizio, J. Raabe, J. Chang, Y. Zhou, W. Zhao, W. Kang, H. Ju, S. Woo, *Nature Electronics* **2020**, *3*, 148.
7. X. Chen, W. Kang, D. Zhu, X. Zhang, N. Lei, Y. Zhang, Y. Zhou, W. Zhao, *Nanoscale* **2018**, DOI 10.1039/C7NR09722K.
8. A. Bogdanov, A. Hubert, *Journal of Magnetism and Magnetic Materials* **1994**, *138*, 255.
9. N. Nagaosa, Y. Tokura, *Nature Nanotechnology* **2013**, *8*, 899.
10. R. Gruber, J. Zázvorka, M. A. Brems, D. R. Rodrigues, T. Dohi, N. Kerber, B. Seng, M. Vafaee, K. Everschor-Sitte, P. Virnau, M. Kläui, *Nature Communications* **2022**, *13*, DOI 10.1038/s41467-022-30743-4.
11. Y. Zhou, M. Ezawa, *Nature Communications* **2014**, *5*, 8.
12. Y. Zhou, E. Iacocca, A. A. Awad, R. K. Dumas, F. C. Zhang, H. B. Braun, J. Åkerman, *Nature Communications* **2015**, *6*, DOI 10.1038/ncomms9193.
13. S.-G. Je, D. Thian, X. Chen, L. Huang, D.-H. Jung, W. Chao, K.-S. Lee, J.-I. Hong, A. Soumyanarayanan, M.-Y. Im, *Nano Letters* **2021**, *21*, 1253.
14. W. Jiang, X. Zhang, G. Yu, W. Zhang, X. Wang, M. Benjamin Jungfleisch, J. E. Pearson, X. Cheng, O. Heinonen, K. L. Wang, Y. Zhou, A. Hoffmann, S. G. E. te Velthuis, *Nature Physics* **2016**, *13*, 162.
15. J. Sampaio, V. Cros, S. Rohart, a Thiaville, a Fert, *Nat Nanotechnol* **2013**, *8*, 839.
16. W. Legrand, D. Maccariello, N. Reyren, K. Garcia, C. Moutafis, C. Moreau-Luchaire, S. Collin, K. Bouzehouane, V. Cros, A. Fert, *Nano Letters* **2017**, *17*, 2703.
17. K. Litzius, I. Lemesh, B. Krüger, P. Bassirian, L. Caretta, K. Richter, F. Büttner, K. Sato, O. A. Tretiakov, J. Förster, R. M. Reeve, M. Weigand, I. Bykova, H. Stoll, G. Schütz, G. S. D. Beach, M. Klaüi, *Nature*

Physics **2017**, *13*, 170.

18. S. Woo, K. Litzius, B. Krüger, M. Y. Im, L. Caretta, K. Richter, M. Mann, A. Krone, R. M. Reeve, M. Weigand, P. Agrawal, I. Lemesh, M. A. Mawass, P. Fischer, M. Kläui, G. S. D. Beach, *Nature Materials* **2016**, *15*, 501.
19. C. Reichhardt, D. Ray, C. J. Reichhardt, *Physical Review Letters* **2015**, *114*, 1.
20. A. Casiraghi, H. Corte-León, M. Vafaee, F. Garcia-Sanchez, G. Durin, M. Pasquale, G. Jakob, M. Kläui, O. Kazakova, *Communications Physics* **2019**, *2*, 1.
21. A. Fernández Scarioni, C. Barton, H. Corte-León, S. Sievers, X. Hu, F. Ajejas, W. Legrand, N. Reyren, V. Cros, O. Kazakova, H. W. Schumacher, *Physical Review Letters* **2021**, *126*, 077202.
22. A. v. Ognev, A. G. Kolesnikov, Y. J. Kim, I. H. Cha, A. v. Sadovnikov, S. A. Nikitov, I. v. Soldatov, A. Talapatra, J. Mohanty, M. Mruczkiewicz, Y. Ge, N. Kerber, F. Dittrich, P. Virnau, M. Kläui, Y. K. Kim, A. S. Samardak, *ACS Nano* **2020**, *14*, 14960.
23. O. Kazakova, R. Puttock, C. Barton, H. Corte-León, M. Jaafar, V. Neu, A. Asenjo, *Journal of Applied Physics* **2019**, *125*, 060901.
24. S. Zhang, J. Zhang, Y. Wen, E. M. Chudnovsky, X. Zhang, *Communications Physics* **2018**, *1*, 36.
25. H. Corte-León, V. Neu, A. Manzin, C. Barton, Y. Tang, M. Gerken, P. Klapetek, H. W. Schumacher, O. Kazakova, *Small* **2020**, 1906144.

Figures

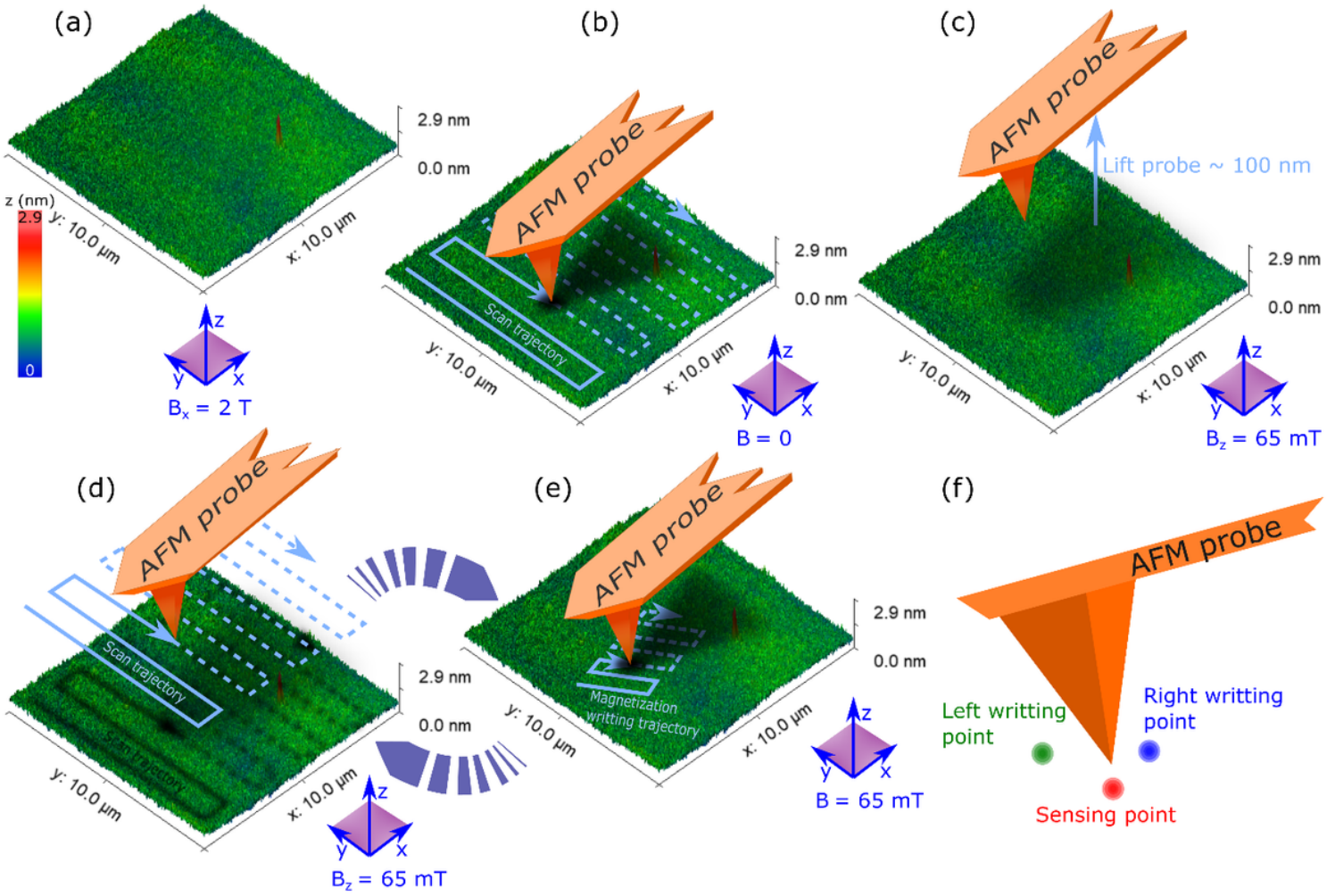

Figure 1

Schematics of the imaging and skyrmions manipulation method used. (a) Sample is exposed to an in-plane field of ~2 T (image shows topography of the surface obtained with AFM). (b) Topography is imaged in semi contact mode without external magnetic field. (c) The probe is lifted from the surface and the out-of-plane magnetic field is increased to 65 mT. (d) MFM imaging is acquired in lift mode with the biasing magnetic field still applied. In lift mode the topography recorded in (b) is used and the probe never moves close to the surface. (e) Magnetization manipulation is performed scanning the area of interest in semi contact mode. (f) Schematics depicting the shift in position between the sensing point of the probe and the writing points.

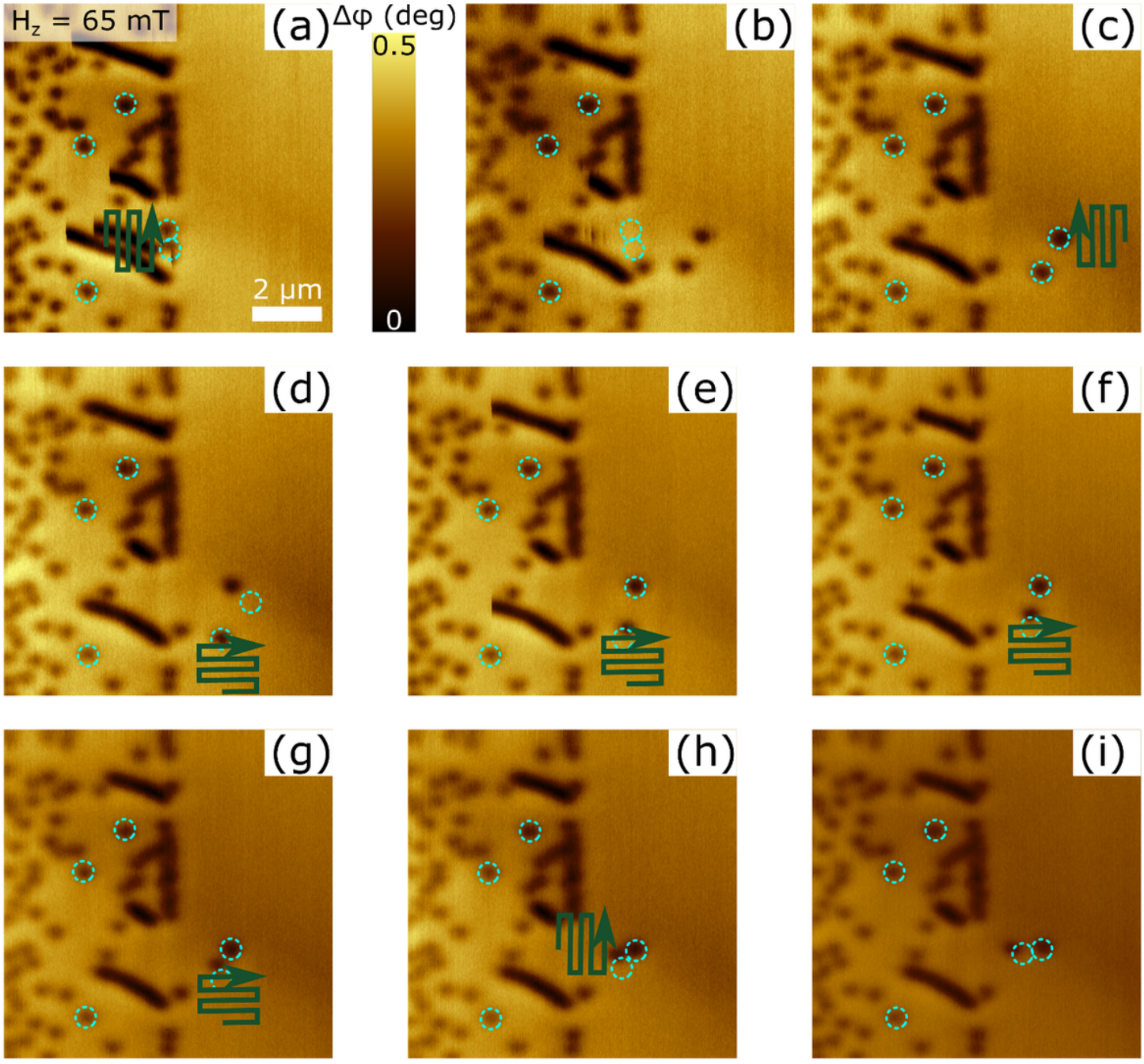

Figure 2

Example of skyrmion collision. (a)-(i) Sequential MFM images showing how several skyrmions are pulled aside, moved to check if they are pinned, brought together, and eventually (h) and (i), they collide. The green arrows indicate the areas where the probe scanned in semicontact mode to manipulate magnetization. The doted circles are guides to mark what changed between images.

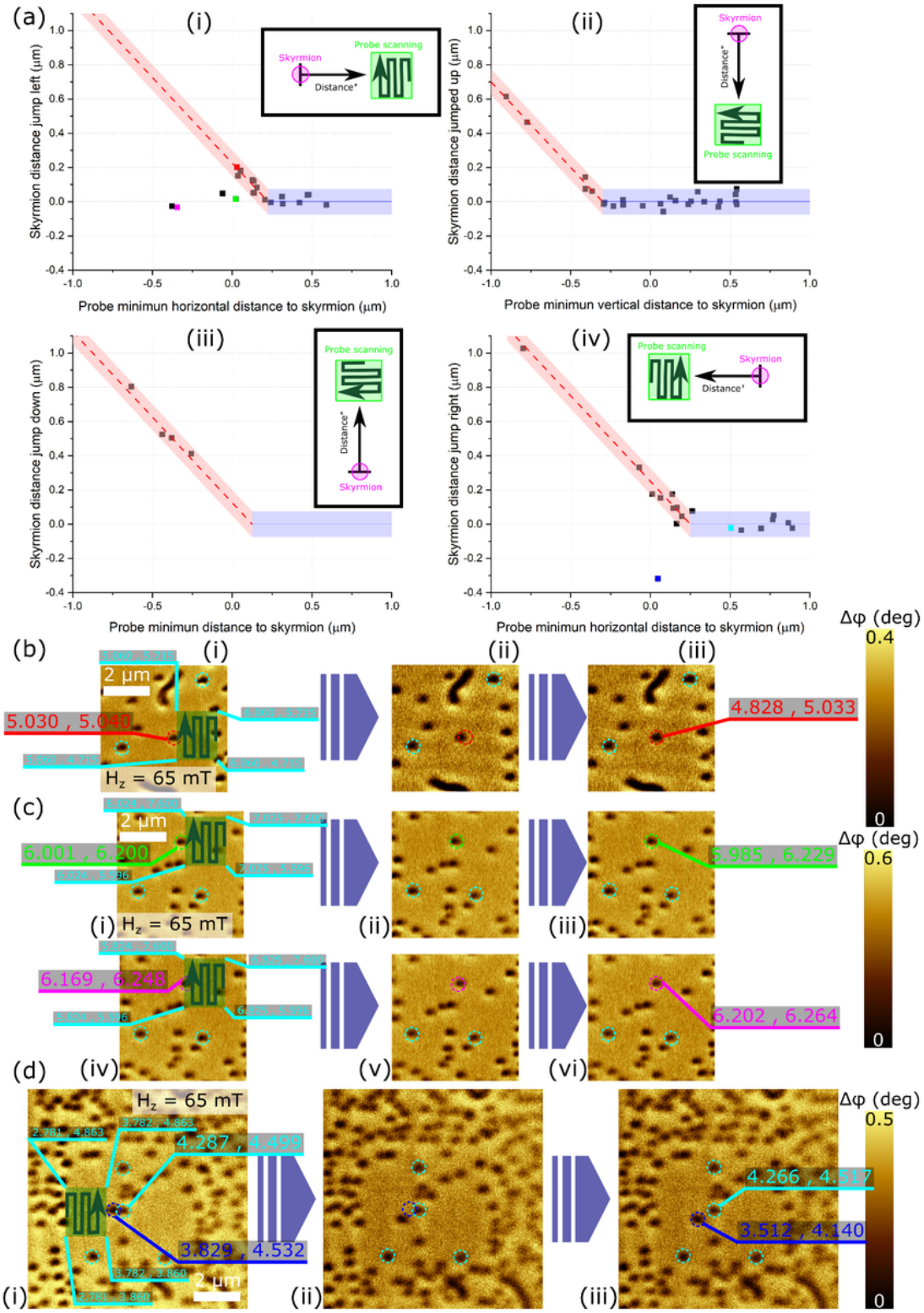

Figure 3

Schematics of the imaging methods used. (a) Topography imaged in semi contact mode without external magnetic field. (b) MFM imaging taken in lift mode with an applied external magnetic field. In lift mode the topography recorded in (a) is used and the probe never moves close to the surface. When writing, not shown here, the probe moves as in (a) with an applied external magnetic field. (c) and (d) are schematic diagrams pretending to show the stray magnetic fields when skyrmions and MFM probe interact. In (c)

with a perfectly symmetrical situation, the sensing point (i.e. where the probe senses the skyrmions) is in between the two points where the field from the probe is large enough to interact with the skyrmions. Note that although close together, the three points do not match. In (d), with a non-symmetrical situation, the left and right writing points have different distance to the sensing point, and thus, when collision experiments are performed, the movement of the skyrmions occurs at different distances depending if the push occurs from the right or the left.

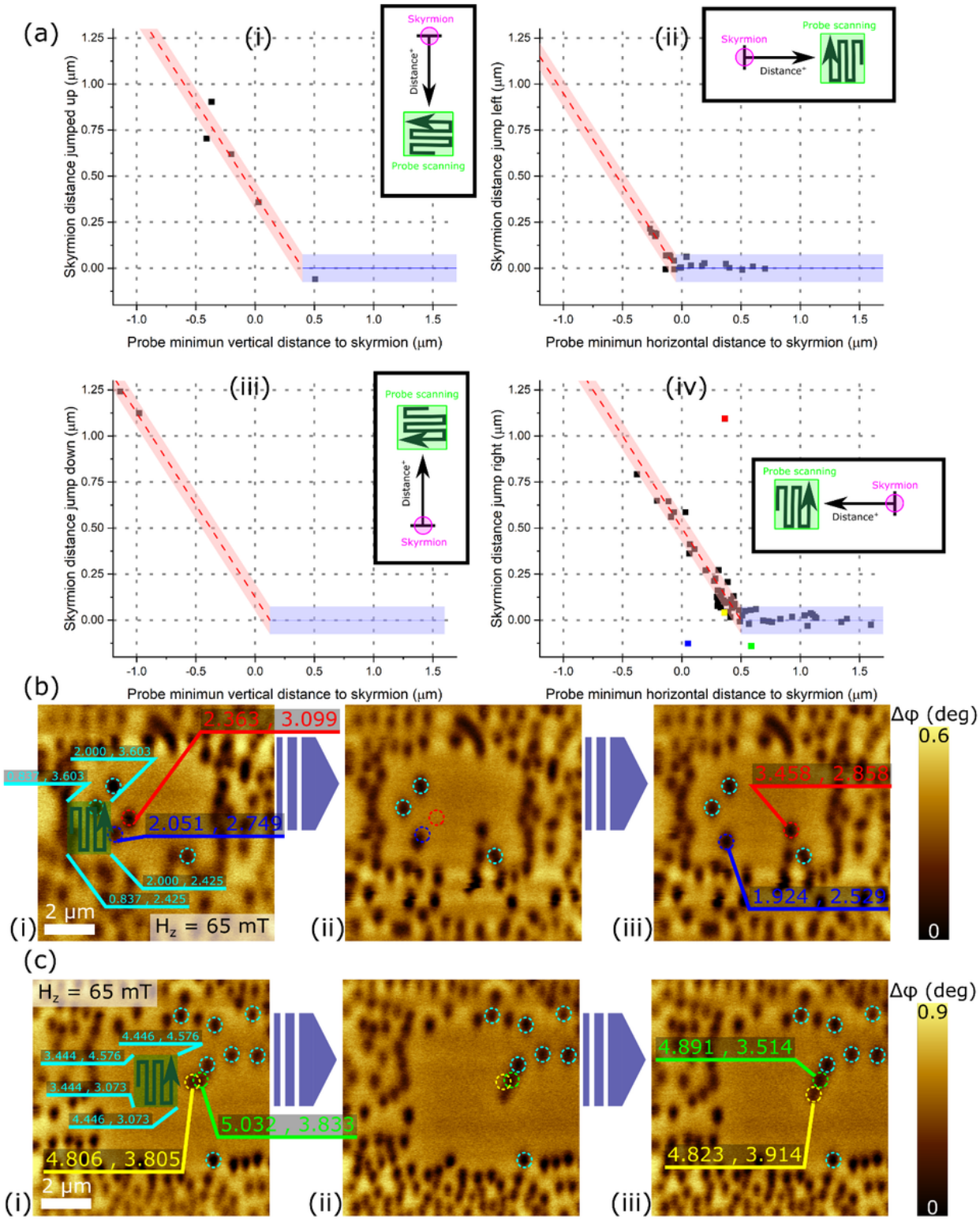

Figure 4

Schematics of the imaging methods used. (a) Topography imaged in semi contact mode without external magnetic field. (b) MFM imaging taken in lift mode with an applied external magnetic field. In lift mode the topography recorded in (a) is used and the probe never moves close to the surface. When writing, not shown here, the probe moves as in (a) with an applied external magnetic field. (c) and (d) are schematic diagrams pretending to show the stray magnetic fields when skyrmions and MFM probe interact. In (c) with a perfectly symmetrical situation, the sensing point (i.e. where the probe senses the skyrmions) is in between the two points where the field from the probe is large enough to interact with the skyrmions. Note that although close together, the three points don’t match. In (d), with a non-symmetrical situation, the left and right writing points have different distance to the sensing point, and thus, when collision experiments are performed, the movement of the skyrmions occurs at different distances depending if the push occurs from the right or the left.

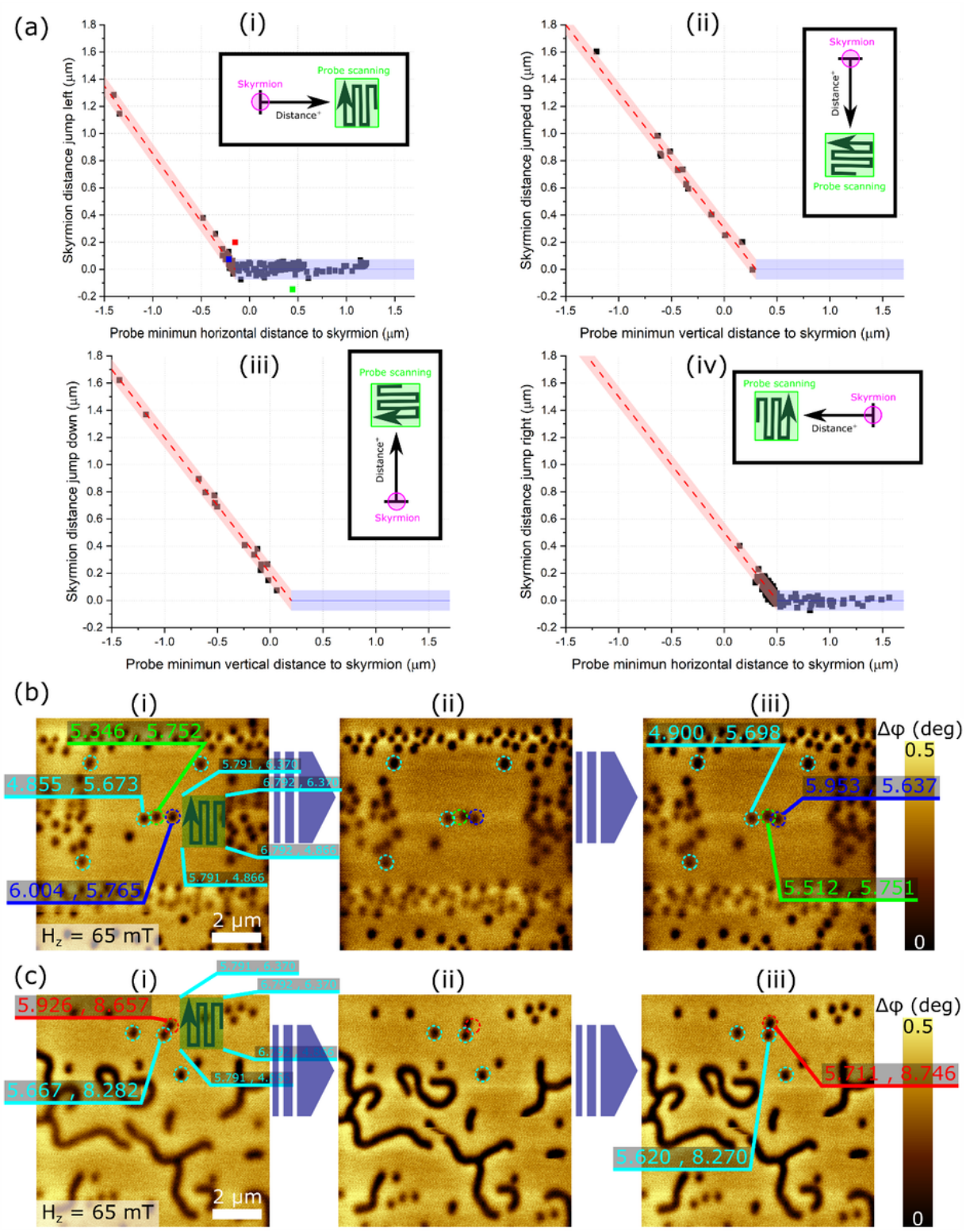

Figure 5

Schematics of the imaging methods used. (a) Topography imaged in semi contact mode without external magnetic field. (b) MFM imaging taken in lift mode with an applied external magnetic field. In lift mode the topography recorded in (a) is used and the probe never moves close to the surface. When writing, not shown here, the probe moves as in (a) with an applied external magnetic field. (c) and (d) are schematic diagrams pretending to show the stray magnetic fields when skyrmions and MFM probe interact. In (c)

with a perfectly symmetrical situation, the sensing point (i.e. where the probe senses the skyrmions) is in between the two points where the field from the probe is large enough to interact with the skyrmions. Note that although close together, the three points do not match. In (d), with a non-symmetrical situation, the left and right writing points have different distance to the sensing point, and thus, when collision experiments are performed, the movement of the skyrmions occurs at different distances depending if the push takes place from the right or the left.

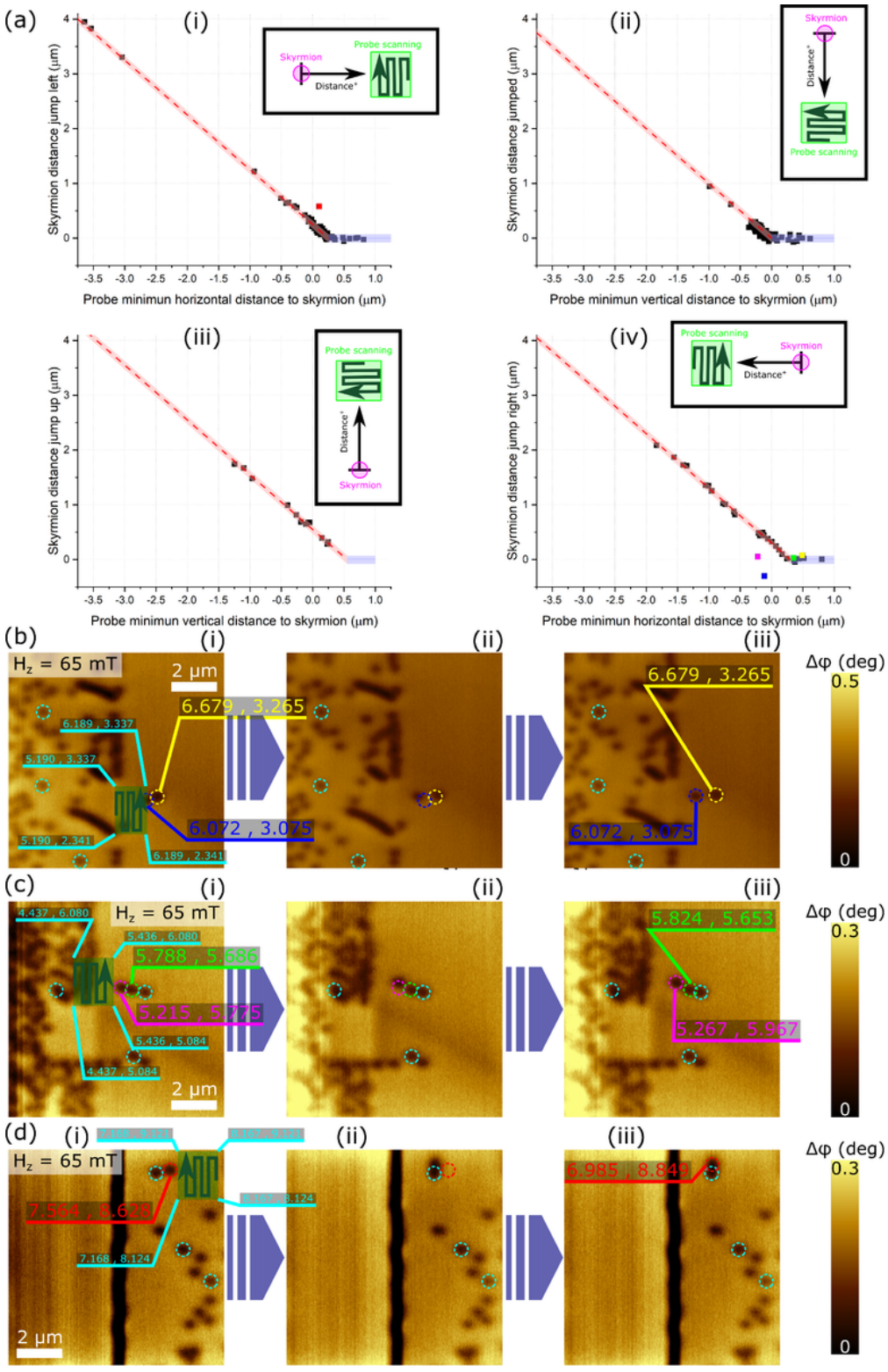

Figure 6

Schematics of the imaging methods used. (a) Topography imaged in semi contact mode without external magnetic field. (b) MFM imaging taken in lift mode with an applied external magnetic field. In lift mode the topography recorded in (a) is used and the probe never moves close to the surface. When writing, not shown here, the probe moves as in (a) with an applied external magnetic field. (c) and (d) are schematic diagrams pretending to show the stray magnetic fields when skyrmions and MFM probe interact. In (c) with a perfectly symmetrical situation, the sensing point (i.e. where the probe senses the skyrmions) is in between the two points where the field from the probe is large enough to interact with the skyrmions. Note that although close together, the three points don't match. In (d), with a non-symmetrical situation, the left and right writing points have different distance to the sensing point, and thus, when collision experiments are performed, the movement of the skyrmions occurs at different distances depending if the push occurs from the right or the left.

Supplementary Files

This is a list of supplementary files associated with this preprint. Click to download.

- mov1.avi
- mov2.avi
- mov3.avi
- mov4.avi
- mov5.avi
- mov6.avi
- mov7.avi
- mov8.avi
- mov9.avi
- mov10.avi
- mov11.avi